applied optics

Fabrication of fast mid-infrared range photodetector based on hybrid graphene–PbSe nanorods

H. Talebi,[1] M. Dolatyari,[2,*] G. Rostami,[2] A. Manzuri,[1] M. Mahmudi,[1] and A. Rostami[1,2,3]

[1]OIC Research Group, University of Tabriz, Tabriz 5166614761, Iran
[2]SP-EPT Laboratories, ASEPE Company, Industrial Park of Advanced Technologies, Tabriz 5364196795, Iran
[3]e-mail: rostami@tabrizu.ac.ir
*Corresponding author: m.dolatyari@gmail.com

Received 27 April 2015; revised 23 May 2015; accepted 23 June 2015; posted 23 June 2015 (Doc. ID 239838); published 10 July 2015

Weak light absorption of graphene has limited the responsivity of graphene-based photodetectors. On the other hand, the slow response of PbSe as a mid-infrared range (MIR) detector makes this type of detector unsuitable as a commercial detector. Here, we report a fast MIR detector based on hybrid graphene–PbSe nanorods. For this purpose, a few-layer graphene piece was synthesized using a simple, scalable, and economical method on a cobalt layer, the synthesized graphene was transferred onto interdigitated copper electrodes, and then synthesized nanorods were spin coated on the transferred graphene. Strong and tunable light absorption in the quantum dot layer creates electric charges, which are transferred to the graphene, and due to the high charge mobility of graphene and long trapped-charge lifetimes in the quantum dot layer, they recirculate many times. The fabricated device has high speed and responsivity. The gain of fabricated detectors based on hybrid graphene quantum dots is 10.3 times more, their response time is 14.3 times faster, and their responsivity is 10 times more than conventional nanorod-based detectors. From the point of view of spectral selectivity, tuning the size of the nanorods helps optical detection from the IR to mid-IR.

OCIS codes: (040.5160) Photodetectors; (040.1880) Detection; (160.4236) Nanomaterials; (160.5140) Photoconductive materials; (160.5335) Photosensitive materials; (260.3060) Infrared.

http://dx.doi.org/10.1364/AO.54.006386

1. INTRODUCTION

Graphene is a two-dimensional sheet/structure of carbon atoms, forming a honeycomb lattice with hybridized bonds, with unique electrical and physical properties [1]. The most interesting electrical properties are high carrier mobility and ballistic transport of charge carriers and half-integer quantum Hall [2–5]. The electrical properties and the low absorbance of graphene make it potentially an ideal transparent conductor where transparency and high conductivity is required [6]. Stiffness, mechanical or flatness stability [7], and high thermal conductivity [8] are the other properties of graphene. These properties have made graphene a suitable candidate for many applications, such as various sensors [9,10], high-frequency transistors [11,12], and optoelectronic applications such as photodetectors [13] and transparent conductive electrodes for solar cells [14] or flat panel displays [15].

So far, the rapid development of graphene-based photodetection has focused on enhancement of the absorption of light in graphene, for example, by exploiting the thermoelectric effects [16–18], metallic plasmonics [19], graphene plasmons [20,21], or microcavities [22,23]. However, the key factor in obtaining ultrasensitive graphene-based photodetection is fabrication of the detector with high gain and the ability to provide multiple electrical carriers per single incident photon. Because of the high transparency of few-layer graphene, the gain is not high in graphene-based photodetectors. Here, we present a new hybrid graphene–PbSe photodetector that exhibits ultrahigh photodetection gain, high quantum efficiency, and high sensitivity. The key functionality of this detector is the application of PbSe nanorods as strong light-absorbers that are spectrally tunable and help facilitate transferring photogenerated charges at higher speeds.

2. EXPERIMENT

A. Synthesis of Graphene

In this experiment, a quartz wafer (5 cm × 2.5 cm) was used as the substrate to deposit 200-nm-thick films of Co by electron beam evaporation. The electron beam evaporation process started when the pressure of the chamber reached below 10^{-6} Torr at 100°C The synthesized Cobalt films were

annealed under a vacuum pressure of 10^{-6} Torr at 500°C or 4 h in a tube furnace. Then the obtained sample was loaded into a sputtering system to deposit solid carbon film on the cobalt thin film. The DC magnetron sputtering system had been evacuated to a base pressure of 3×10^{-6} Torr, and the sputtering was done at a working pressure of 10^{-4} Torr and an Ar pressure of 25 SCCM. The thickness of the carbon layer was recorded as 2 nm. Thermal annealing of the amorphous carbon was performed for the synthesis of graphene in a tube furnace at 900°C under high vacuum for 45 min. The graphene was transferred onto interdigitated electrodes using a polymethyl methacrylate (PMMA) layer. In this process PMMA was spin coated on the graphene film grown on Co/quartz and cured at 180°C. Then wafer was dipped into a nitric acid and hydrofluoric acid solution (1:1) at room temperature. In this case, the etching rate was 30 and 20 Å per second for cobalt and quartz, respectively, and after 5 h, when the Co layer was completely removed and the quartz substrate partially etched (thickness of about 36 μm), the detached graphene film was placed in a water bath. The PMMA/graphene film was washed with deionized water and placed on the interdigitated electrodes and dried, and then the PMMA was dissolved by acetone.

B. Synthesis of PbSe Nanorods

Pb(Ac)2 (1 mmol) was dissolved in oleylamine (OLA) (10 ml) in a 250 ml three-neck flask under vacuum. Selenium (1 mmol) and sodium borohydride (0.1 g) were dissolved in 5 ml of 2-propanol and injected at a temperature of 110°C into the Pb(Ac)2–OLA gel. The temperature was stabilized at 110°C for 20 min during the growth. The precipitate was redispersed in hexane and then washed several times with ethanol and 2-propanol and dried at 50°C for 2 h. To exchange the surface coordinated OLA with thioacetamide (TAA), 15 mg of synthesized PbSe and 30 mg of TAA were dispersed in 20 ml of 2-propanol and stirred for 18 h at room temperature. The solution was centrifuged at 6000 rpm for 10 min, and precipitate was redispersed in 2-propanol and washed five times with ethanol and 2-propanol. The obtained material was spin coated on graphene transferred onto interdigitated electrodes, and the device was dried at 100°C for 12 h.

C. Characterization

X-ray diffraction (XRD) (Siemens D500 instrument) of the graphene and PbSe samples was recorded from 2° to 70°. The thickness and morphology of the prepared graphene were determined by an atomic force microscope (dual scope c-26 scanning probe and optical microscope), and the nanostructure of quantum dot (QD) samples was observed by field emission scanning electron microscopy (SEM; Tescan model MIRA3). UV/visible absorption spectra of the samples were recorded by employing a PG Instruments Ltd. T70 UV/visible spectrophotometer.

3. RESULTS AND DISCUSSION

The broad (002) peak at $2\theta = 22°$ can be detected in Fig. 1, which depicts an interlayer distance of 0.4 nm according to the Bragg relation ($2d \sin \theta = n\lambda$). This is 0.334 nm in graphite, and it indicates the complete exfoliation and destruction of the ordered layered structure of graphite.

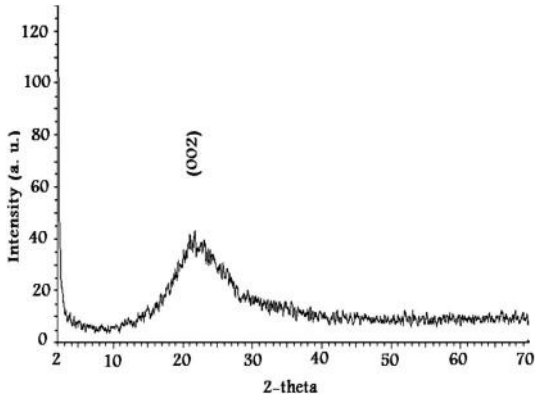

Fig. 1. XRD pattern of the synthesized graphene.

The XRD pattern of the PbSe nanorods was indexed to a cubic phase with lattice parameters of $a = 6.05$ Å (Fig. 2). The intensity and positions of the peaks are in good agreement with the values reported in the literature (JCPDS 05–0592). All the diffraction peaks could be indexed to (111), (200), (220), (311), (222), (400), (331), and (420) reflections of the face-centered cubic PbSe structure. With reduction of the crystalline size toward the nanometer scale, a broadening in the diffraction peaks is observed, and the width of the peak directly correlates to the size of the nanocrystalline domain due to the Debye–Scherrer relation. The size of the synthesized nanoparticles is estimated to be about 28 nm by the Debye–Scherrer relation.

Figure 3 presents the Fourier transform IR (FT-IR) spectrum of PbSe nanorods and graphene. The spectrum [Fig. 3(a)] confirms the existence of absorption bands in the range 3–5 μm for PbSe nanorods. Also, weak absorption bands for graphene can be observed in the range 3–5 μm [Fig. 3(b)]. The sheet resistance of the synthesized graphene is 2 kΩ/sq. Figure 4 shows the topology of synthesized graphene using atomic force microscopy (AFM). As seen in the AFM image, the thickness of the synthesized graphene layer is about 2 nm, and the deposited layer is almost homogenous.

The SEM image of the PbSe nanorods is displayed in Fig. 5 and shows that the morphology of the synthesized materials is rodlike. The average size of the materials is about 50 nm.

The device is fabricated with a graphene sheet, which is transferred onto interdigitated electrodes and sensitized by

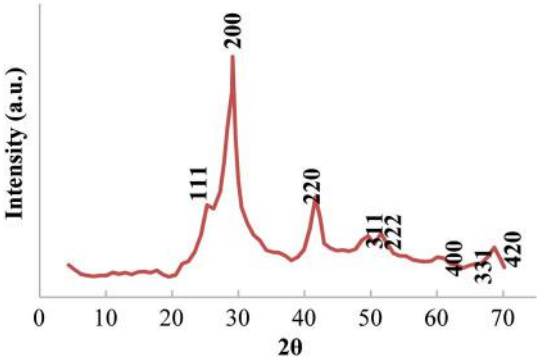

Fig. 2. XRD pattern of the synthesized PbSe Nanorods.

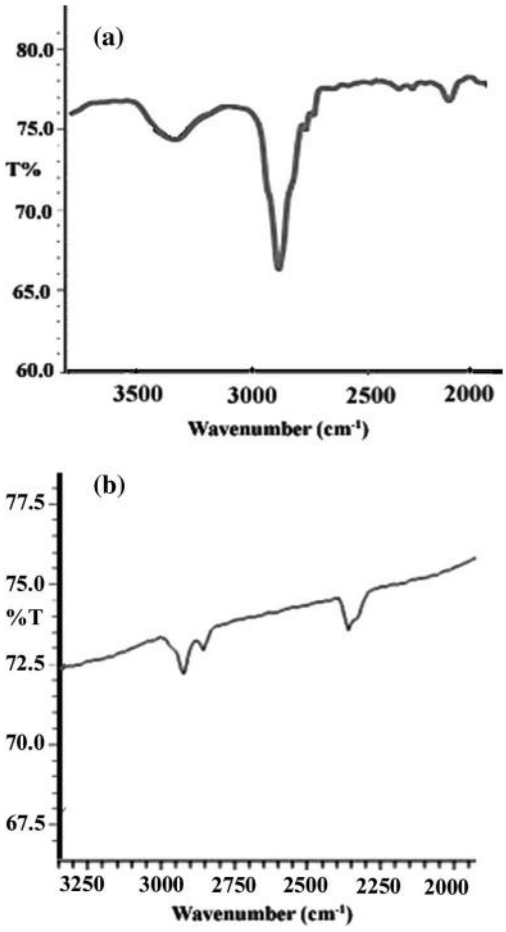

Fig. 3. FT-IR spectrum of the synthesized (a) PbSe nanorods and (b) graphene.

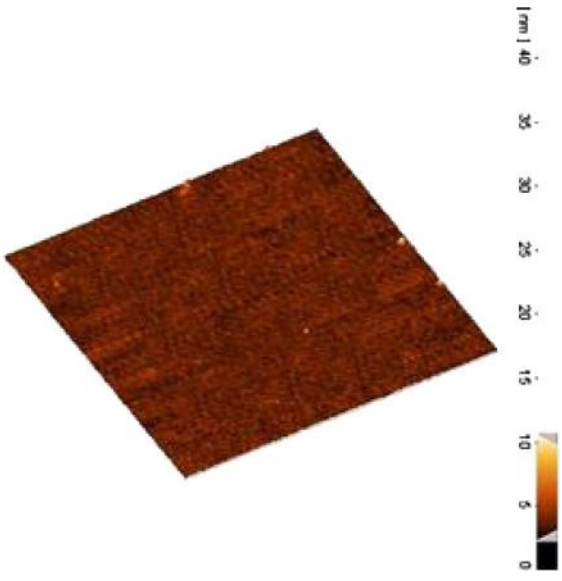

Fig. 4. Typical atomic force microscopy image of the synthesized graphene.

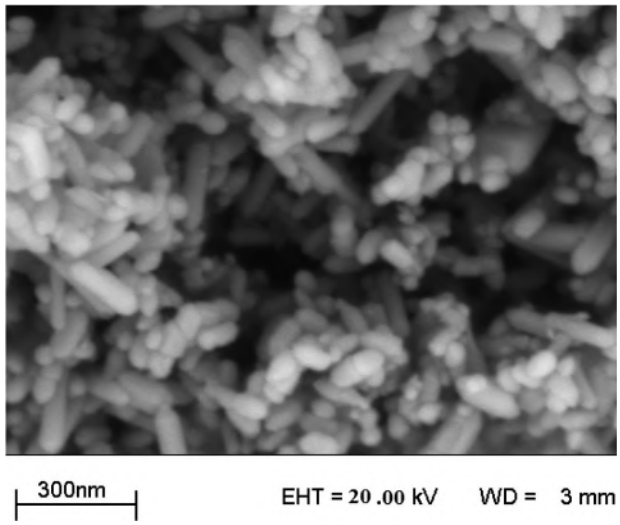

Fig. 5. SEM image of the synthesized PbSe nanorods.

PbSe nanomaterials. Graphene is the carrier transport channel, and the nanorods are used as the photon absorbing material [24]. Konstantatos *et al.* have published similar research work in which graphene decorated with PbS QDs on top of a silicon/SiO_2 wafer has been used for fabrication of a phototransistor [24]. They have proved that the graphene provides a gate-tunable carrier density and polarity that enable tuning of the sensitivity of the transistor and increase its speed. PbS QDs act as near-IR absorber at a range of 1–3 μm, and operation of their hybrids with thiols as photodetectors without graphene is relatively fast. In this study PbSe is used for operation at 3–5 μm wavelengths. PbSe does not have a fast response, and here we improved its operation with TAA passivation and the improved material applied on the graphene that was on the interdigitated electrodes for fabrication of the mid-IR range (MIR) photodetector. In contrast to what has been shown previously in graphene-based detectors, where photocurrent generation occurs at the interface of graphene and metal contacts, or in the vicinity of a p–n junction, these structures are photoresponsive over a large area, a feature of importance in most sensing applications [24]. In our structure graphene is used on the interdigitated electrodes. Here electrons can inject from the electrode to the graphene, and then they can transfer from the graphene to the nanorods. Electrons can be tunneled between rods and then they can transfer to another electrode.

The fabricated device based on PbSe nanorods capped by the OLA ligand do not show sensitivity on IR illumination ($\lambda = 3$ μm), which is possibly related to the long chain of OLA. By replacing OLA with TAA, the photosensitivity of the detector becomes higher. Figure 6(a) depicts I–V characteristics of the photodetector device fabricated based on PbSe nanorods capped by TAA both in the dark and under IR illumination ($\lambda = 3$ μm). Applying graphene under nanorods causes an increase in the dark current and photocurrent [Fig. 6(b)], which indicates high responsivity and low sensitivity of the fabricated device based on graphene nanorods.

With a bias voltage of 5 V, the detector based on TAA-capped PbSe nanorods demonstrates a dark current density

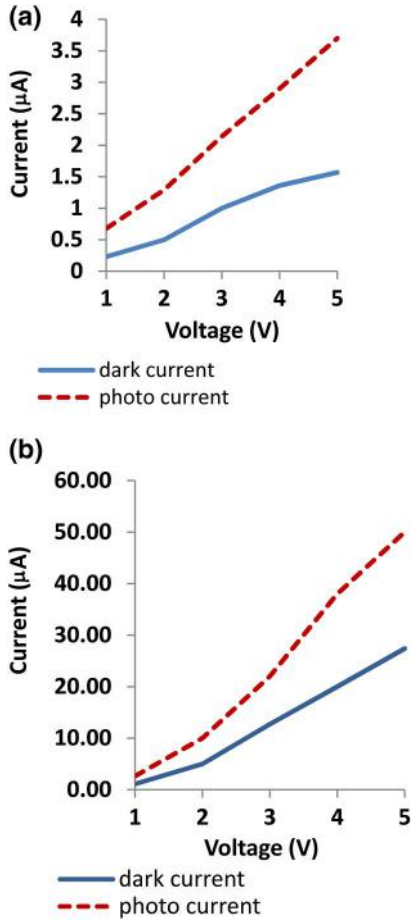

Fig. 6. I–V characteristics of the fabricated detectors based on the synthesized (a) PbSe–TAA nanorods and (b) hybrid graphene–PbSe–TAA nanorods under IR illumination with a power of 6.6 μW (λ = 3–5 μm).

of 1.5 μAmm^{-2} and photocurrent density of 3.7 μAmm^{-2} [Fig. 6(a)]. Also, in the same conditions, a dark current density of 27.40 μAmm^{-2} and photocurrent density of 50 μAmm^{-2} are observed for the device based on hybrid graphene–PbSe nanorods capped with TAA [Fig. 6(b)]. The results indicate that hybrid graphene–PbSe increases responsivity by a factor of 15.

The photosensitivity of a detector (S) can be described by $S = (R_i - R_d)/R_i$, where R_d and R_i are the electrical resistance in the dark and under IR illumination, respectively [25]. The photosensitivity of the fabricated detectors is calculated to be 1.47 and 0.82 for PbSe nanorods capped with TAA and hybrid graphene-based TAA-capped PbSe, respectively. According to the results obtained, the photosensor fabricated using TAA-passivated nanorods exhibits high sensitivity over a large variation in bias. Furthermore, photoconductive gain (G) is defined as the ratio of the number of electrons collected per unit time to the number of photons absorbed per unit time [25]. By applying responsivity values of 0.56 and 7.6 AW^{-1} (for a source with power of 6.6 μW and 5 V bias voltage) and wavelength of 3 μm to the expression, the estimated gain of the devices based on PbSe nanorods passivated by TAA is 0.3, and it increases to 3.1 when graphene is used as a carrier channel in these structures.

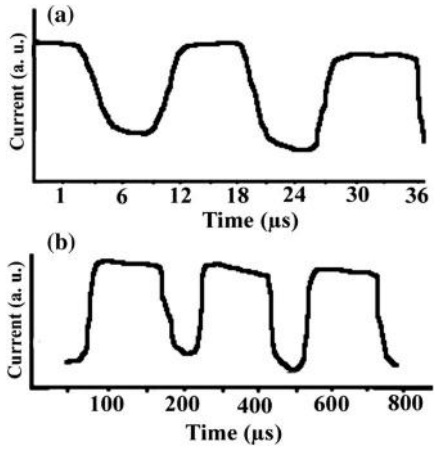

Fig. 7. Photocurrent transient response of fabricated detectors based on (a) PbSe–TAA and (b) hybrid graphene–PbSe–TAA under illumination of light with a wavelength of 3 μm and power of 3×10^{-6} W/cm^2.

The device made using PbSe–TAA exhibits a rise time of 400 μs [Fig. 7(a)], and this time for the graphene-based detector is 28 μs. The results show the response time of the graphene-based detector is 14.3 times faster than the PbSe–TAA detector. In fact, graphene is the carrier transport channel, and the nanorods are used as the photon absorbing material in this work. The response time measurement was performed using IR light illumination and an optical chopper with a stable rotating speed that periodically interrupted the light beam. The chopper wheel was mounted in front of the detector, and the photodetector response time was measured when illuminated with discontinuous 3–5 μm IR light at a maximum motor speed of 1 kHz [26].

4. CONCLUSION

In this work, PbSe nanorods passivated by OLA ligands were synthesized by a thermal decomposition method. The long-tailed OLA ligands were exchanged for shorter TAA ligands. A few-layer graphene piece was prepared by the sputtering method, and the prepared materials were used for fabrication of the MIR detectors. The results illustrate that the detector fabricated from hybrid graphene–PbSe nanorods shows a fast response with high responsivity. The gain of detectors fabricated based on hybrid graphene nanorods is 10.3 times more, their response time is 14.3 times faster, and their responsivity is 10 times more than conventional nanorod-based detectors.

REFERENCES

1. M. I. Katsnelson, "Graphene: carbon in two dimensions," Mater. Today **10**(1–2), 20–27 (2007).
2. A. K. Geim and K. S. Novoselov, "The rise of graphene," Nat. Mater. **6**, 183–191 (2007).
3. A. H. C. Neto, F. Guinea, N. M. R. Peres, K. S. Novoselov, and K. Geim, "The electronic properties of graphene," Rev. Mod. Phys. **81**, 109–162 (2009).
4. I. Meric, M. Y. Han, A. F. Young, B. Ozyilmaz, P. Kim, and K. L. Shepard, "Current saturation in zero-bandgap, top-gated graphene field-effect transistors," Nat. Nanotechnol. **3**, 654–659 (2008).

5. Y. Zhang, Y. W. Tan, H. L. Stormer, and P. Kim, "Experimental observation of the quantum Hall effect and Berry's phase in graphene," Nature **438**, 201–204 (2005).
6. F. Bonaccorso, Z. Sun, T. Hasan, and A. C. Ferrari, "Graphene photonics and optoelectronics," Nat. Photonics **4**, 611–622 (2010).
7. J. Hone, C. Lee, X. D. Wei, and J. W. Kysar, "Measurement of the elastic properties and intrinsic strength of monolayer graphene," Science **321**, 385–388 (2008).
8. A. A. Balandin, S. Ghosh, W. Bao, I. Calizo, D. Teweldebrhan, F. Miao, and C. N. Lau, "Superior thermal conductivity of single-layer graphene," Nano Lett. **8**, 902–907 (2008).
9. J. D. Fowler, M. J. Allen, V. C. Tung, Y. Yang, R. B. Kaner, and B. H. Weiller, "Practical chemical sensors from chemically derived graphene," ACS Nano. **3**, 301–306 (2009).
10. C. Shan, H. Yang, J. Song, D. Han, A. Ivaska, and L. Niu, "Direct electrochemistry of glucose oxidase and biosensing for glucose based on graphene," Anal. Chem. **81**, 2378–2382 (2009).
11. Y. Wu, Y. M. Lin, A. A. Bol, K. A. Jenkins, F. Xia, D. B. Farmer, Y. Zhu, and P. Avouris, "High-frequency, scaled graphene transistors on diamond-like carbon," Nature **472**, 74–78 (2011).
12. J. Svensson, N. Lindahl, H. Yun, M. Seo, D. Midtvedt, Y. Tarakanov, N. Lindvall, O. Nerushev, J. Kinaret, S. W. Lee, and E. E. B. Campbell, "Carbon nanotube field effect transistors with suspended graphene gates," Nano Lett. **11**, 3569–3575 (2011).
13. F. Xia, T. Mueller, Y.-M. Lin, A. Valdes-Garcia, and P. Avouris, "Ultrafast graphene photodector," Nat. Nanotechnol. **4**, 839–843 (2009).
14. X. Wang, L. Zhi, and K. Mullen, "Transparent, conductive graphene electrodes for dye-sensitized solar cells," Nano Lett. **8**, 323–327 (2008).
15. S. Bae, H. Kim, Y. Lee, X. Xu, J.-S. Park, Y. Zheng, J. Balakrishnan, T. Lei, H. R. Kim, Y. I. Song, Y.-J. Kim, K. S. Kim, B. Ozyilmaz, J.-H. Ahn, B. H. Hong, and S. Iijima, "Roll-to-roll production of 30-inch graphene films for transparent electrodes," Nat. Nanotechnol. **5**, 574–578 (2010).
16. M. Lemme, "Gate-activated photoresponse in a graphene p-n junction," Nano Lett. **11**, 4134–4137 (2011).
17. N. M. Gabor, "Hot carrier-assisted intrinsic photoresponse in graphene," Science **334**, 648–652 (2011).
18. J. C. W. Song, M. S. Rudner, C. M. Marcus, and L. S. Levitov, "Hot carrier transport and photocurrent response in graphene," Nano Lett. **11**, 4688–4692 (2011).
19. T. J. Echtermeyer, "Strong plasmonic enhancement of photovoltage ingraphene," Nat. Commun. **2**, 458 (2011).
20. F. H. L. Koppens, D. E. Chang, and F. J. Garcıa de Abajo, "Graphene plasmonics: a platform for strong light-matter interactions," Nano Lett.. **11**, 3370–3377 (2011).
21. S. Thongrattanasiri, F. H. L. Koppens, and F. J. Garcia de Abajo, "Complete optical absorption in periodically patterned graphene," Phys. Rev. Lett. **108**, 047401 (2012).
22. M. Furchi, "Microcavity-integrated graphene photodetector," 2011, http://arXiv.org/abs/1112.1549.
23. M. Engel, "Light–matter interaction in a microcavity-controlled graphene transistor," 2011, http://arXiv.org/abs/1112.1380.
24. G. Konstantatos, M. Badioli, L. Gaudreau, J. Osmond, M. Bernechea, F. Pelayo, G. Arquer, F. Gatti, and F. H. L. Koppens, "Hybrid graphene-quantum dot phototransistors with ultrahigh gain," Nat. Nanotechnol. **7**, 363–368 (2012).
25. S. Miri, A. Rostami, M. Dolatyari, H. Baghban, H. Rasooli, and E. Amini, "Fabrication of fast and sensitive IR-detectors based on PbS quantum dots passivated by organic ligands," Phys. Status Solidi A **210**, 420–424 (2013).
26. F. Jabbarzadeh, M. Siahsar, M. Dolatyari, and G. Rostami, "Fabrication of new mid-infrared photodetectors based on graphene modified by organic molecules," IEEE Sens. J. **15**, 2795–2800 (2015).